

A simple spatiotemporal chaotic Lotka-Volterra model

J. C. Sprott^{*}, J. C. Wildenberg

*Department of Physics, University of Wisconsin, Madison, Wisconsin 53706
USA*

Yousef Azizi

Institute for Advanced Studies in Basic Sciences, Zanjan, Iran

Abstract

A mathematically simple example of a high-dimensional (many-species) Lotka-Volterra model that exhibits spatiotemporal chaos in one spatial dimension is described. The model consists of a closed ring of identical agents, each competing for fixed finite resources with two of its four nearest neighbors. The model is prototypical of more complicated models in its quasiperiodic route to chaos (including attracting 3-tori),

^{*}Corresponding author. Tel.: +1-608-263-4449; fax: +1-608-262-7205

E-mail addresses: sprott@physics.wisc.edu (J. C. Sprott), jcwildenberg@wisc.edu (J. C. Wildenberg), joseph_azizi@yahoo.com (Yousef Azizi).

bifurcations, spontaneous symmetry breaking, and spatial pattern formation.

1. Introduction

The Lotka-Volterra model [1,2] is widely used to study the dynamics of interacting species in ecology and elsewhere [3] and has even been implemented with analog electronics [4]. One form of such a system has N species (or agents) with population x_i for $i = 1$ to N that compete for a fixed finite set of resources according to

$$\frac{dx_i}{dt} = r_i x_i \left(1 - \sum_{j=1}^N a_{ij} x_j \right) \quad (1)$$

where r_i is the linear growth rate of the i^{th} species, and a_{ij} is the extent to which species j competes for the resources of species i . Equation (1) can be viewed as the first approximation in a Taylor-series expansion for a wide class of nonlinear models [5] with the highly desirable feature that solutions are asymptotically bounded ($0 \leq x_i \leq 1$) when $a_{ij} \geq 0$. The biologically realistic and most interesting examples of Eq. (1) have chaotic solutions for very large N with sparse a_{ij} matrices whose nonzero elements correspond to spatially nearby neighbors.

An exhaustive numerical search suggests that the simplest such example is of the form

$$\frac{dx_i}{dt} = x_i (1 - ax_{i-2} - x_i - bx_{i+1}) \quad (2)$$

in which all species are identical and the boundary conditions are periodic ($x_{-1} = x_{N-1}$, $x_0 = x_N$, and $x_{N+1} = x_1$). Equation (2) is a simple example of a circulant a_{ij} matrix [6]. Setting

$r_i = 1$ and $a_{ii} = 1$ does not sacrifice any generality since it corresponds to measuring time in units of the inverse growth rate of the (identical) species and x in units of the carrying capacity of each species in the absence of the others. In this paper we take $a = b = s$, for which chaos occurs at $s = 1$ provided N is sufficiently large. The quantity s is a useful bifurcation parameter that measures the coupling between species, with $s = 0$ corresponding to the system decoupling into N independent Verhulst equations [7] whose solutions are asymptotic to $x_i = 1$ for all i , and $s \rightarrow \infty$ corresponding to severe competition in which only a single species survives.

This system has 2^N equilibria of which only the one with $x_i = 1/(a + b + 1)$ for all i corresponds to coexistence. The coexisting equilibrium has all x_i positive, and the system is dissipative for $a + b > -1$ with a rate of state-space contraction given by $-N/(a + b + 1)$ for $N > 2$. Thus for $s > -0.5$, we expect the system to have attractors, as appears to be the case from numerical tests.

The complex eigenvalues of the coexisting equilibrium with $N = 100$ and $s = 1$ are shown in Fig. 1. The trefoil shape is typical of other values of N and s . This case has 16 unstable directions (eigenvalues with positive real parts), two neutral directions (real parts that are zero) with a frequency of $\omega = 1/3$, and 82 stable directions (real parts that are negative). All but two of the eigenvalues (at -1 and $-1/3$) are complex conjugate pairs. Thus the equilibrium for this case is an index-16 spiral saddle. Animated versions of Fig. 1 with $s = 0.888$ (near the Hopf bifurcation point) and N varying from 1 to 300, and with $N = 100$ and s varying from 0 to 1.15 are available on the Web [8].

This system can be considered as a homogeneous one-dimensional ring of identical agents, each experiencing competition from its nearest neighbor on the right and from its second nearest neighbor on the left as shown in Fig. 2. While this behavior is perhaps not very biologically realistic, the resulting dynamics share many of the features of more complicated and hence more realistic heterogeneous models, and thus it warrants study because of its elegant simplicity and apparent generality.

2. Routes to Chaos

The system in Eq. (2) provides an opportunity to explore the routes to chaos in a high-dimensional spatial Lotka-Volterra model. For $s = 1$ and $1 \leq N \leq 100$, the route is conveniently quantized as indicated in Fig. 3, which shows the largest Lyapunov exponent λ_1 [9] and the Kaplan-Yorke dimension D_{KY} [10]. The largest Lyapunov exponent is a measure of the sensitivity to initial conditions, with a positive value signifying chaos. The dimension is a measure of the complexity of the attractor or the number of active variables, with integer values corresponding to periodicity (for $D_{KY} = 1$) or quasiperiodicity (for $D_{KY} \geq 2$) and noninteger values corresponding to strange (fractal) attractors [11,12]. From this information as well as calculations of the eigenvalues of the coexisting equilibrium, state-space plots, and Poincaré sections, the attractor type has been identified and catalogued in Table I. The route is a rather complicated sequence of quasiperiodic solutions with equilibria, limit cycles, 2-tori, and 3-tori prior to the onset of chaos. In this table and the graphs that follow, the equations were solved using a fourth-

order Runge-Kutta method with a fixed step size of 0.05, although most of the quoted values were confirmed using a step size of 0.01.

Some of the N values (3, 4, 6, 8, 9, and 12) happen to lie exactly on Hopf bifurcation points [13] as evidenced by pairs of complex eigenvalues with zero real parts. The ones at $N = 4$ and 8 have imaginary parts of $\omega = 1/3$. The one at $N = 12$ has two pairs of complex eigenvalues with zero real parts and $\omega = 1/3$ and $1/\sqrt{3}$, and thus it is a Hopf-Hopf, codimension-2 bifurcation. The ones at $N = 3, 6,$ and 9 are attractors in $N - 2$ dimensions of the state space, but are invariant loops (neutrally stable) in the remaining two dimensions, with an amplitude that depends on the initial conditions and a linear frequency $\omega = 1/\sqrt{3}$.

The case $N = 16$ is an especially simple and elegant example of an attracting 3-torus in an autonomous dissipative system [14,15]. The case $N = 54$ is a highly crinkled 3-torus, very close to the onset of chaos. The absence of 4-tori is consistent with the theorem of Ruelle and Takens [16], which states that such systems are structurally unstable with respect to arbitrarily small C^∞ perturbations, whereas 3-tori are unstable only for C^2 perturbations. A C^k perturbation is one whose derivatives up to order k are less than ε for any ε .

Chaos onsets at $N = 59$ followed by several quasiperiodic windows (3-tori) before becoming permanently chaotic for $N \geq 66$, with a very slowly increasing largest Lyapunov exponent and a linearly increasing attractor dimension. For $N = 100$, the largest Lyapunov exponent is $\lambda_1 \cong 0.00777$, and the Kaplan-Yorke dimension is $D_{KY} \cong$

11.3171. The system with $N = 100$ is hyperchaotic with four positive Lyapunov exponents, whose sum $K = \sum_{k=1}^4 \lambda_k \cong 0.0164$ is a measure of the entropy [17].

For larger N , the Lyapunov exponent appears to saturate at a value around $\lambda_1 \cong 0.01$, while the Kaplan-Yorke dimension continues to increase linearly. A linear least-squares fit over the range $71 \leq N \leq 104$ gives $D_{KY} = 0.1356N - 2.25$. If this scaling holds for arbitrarily large N , the system provides a simple method for producing a strange attractor with a rather precisely controlled high dimension. The dimension of the attractor is approximately equal to the number of unstable eigenvalues of the coexisting equilibrium as shown in Fig. 1. Chaos also occurs for values of N as small as 7 with $s = 1.4$, for which $\lambda_1 \cong 0.00315$ and $D_{KY} \cong 3.255$, and for $N = 10$ with $s = 1.3$, for which $\lambda_1 \cong 0.00316$ and $D_{KY} \cong 3.659$.

This general route to chaos is typical of other similar high-dimensional systems, including fully-connected Lotka-Volterra models and artificial neural networks [18,19], and it is not sensitive to the chosen bifurcation parameter. For example, holding N fixed at 100 and varying s gives a quasiperiodic route as shown in Fig. 4. In this case, the first Hopf bifurcation occurs at $s \cong 0.888916012261$, and chaos onsets at $s \cong 0.916$. For values of N greater than 100, the value of s at which the Hopf bifurcation occurs oscillates slightly but appears to asymptote to a value close to the value at $N = 100$ in the limit of large N . Similarly, the onset of chaos appears to asymptote to a value of about $s \cong 0.90$ in the limit of large N , although this detail warrants further study.

For $N = 100$, there is a quasiperiodic window spanning the approximate range $1.1047 < s < 1.1151$. For $s = 1.11$, the attractor appears to be a crinkled 3-torus from the double Poincaré section, and there are three Lyapunov exponents that are very close and oscillating about zero, with two others that are very small but apparently slightly negative, in addition to the 95 that are significantly negative. The quasiperiodic attractor apparently coexists with a chaotic one and has a relatively small basin of attraction. This window disappears as N increases. In this figure, s is increased slowly without reinitializing the variables for each new s , and thus the plot is not unique because of the existence of multiple attractors for some values of s , especially near the onset of chaos.

The case with $N = 10$ also exhibits a quasiperiodic route to chaos with increasing s , progressing from an equilibrium to a limit cycle (with a Hopf bifurcation at $s \cong 0.894427191$) to a 2-torus to chaos at $s \cong 1.25$. This route to chaos is very different from that observed in most low-dimensional systems such as the logistic map and the Lorenz attractor, where the period-doubling route to chaos is common, although it sometimes occurs in low-dimensional systems such as the time-delayed logistic map [20]. The route is a consequence of the trefoil shape of the eigenvalue spectrum as shown in Fig. 1, in which the first eigenvalues to become unstable are necessarily a complex conjugate pair.

3. Spatiotemporal Patterns

Initial conditions with all x_i identical and positive have solutions that attract to the equilibrium at $x_i = 1/(a + b + 1)$. For $a = b = 1$ and $N = 100$, these points lie on an 82-

dimensional stable manifold of the saddle point equilibrium, which is nevertheless a set of measure zero in the 100-dimensional state space. Most other initial conditions approach a strange attractor for $s = 1$ and $N \geq 66$.

Figure 5 shows a spatiotemporal plot of the attractor for $s = 1$ and $N = 480$, in which the value of $|x_{i+1} - x_i|$ is plotted at each point using a 16-level gray scale with black corresponding to zero and white to 1.0. The quantity plotted was chosen because it well exhibits the spatiotemporal structure and suppresses the small-scale spatial periodicity that results from adjacent neighbors tending to oscillate with opposite phase. There are obvious structures that propagate in the $+i$ direction with a typical velocity of the order $di/dt \cong 1/8$.

This plot illustrates spontaneous symmetry breaking [21-23] since spatially heterogeneous solutions occur in a system whose equations are spatially homogeneous. The structure is not a remnant of the random initial conditions and occurs even for highly ordered initial conditions off the stable manifold. Such plots offer a lesson to ecologists and others who instinctively assume that there must be a cause for the particular spatial heterogeneities observed in natural systems.

By contrast, spatiotemporal plots (not shown) for cases that are temporally periodic (such as $N = 100$ and $s = 0.9$ where the solution is a limit cycle), exhibit spatial periodicity with propagating waves.

Another way to view the spatiotemporal structure is through the spatiotemporal cross-correlation function

$$C(\Delta i, \Delta t) = \frac{\left| \int [x_{N/2}(t) - \bar{x}][x_{N/2+\Delta i}(t + \Delta t) - \bar{x}] dt \right|}{\int [x_{N/2}(t) - \bar{x}]^2 dt} \quad (3)$$

where

$$\bar{x} = \lim_{T \rightarrow \infty} \frac{1}{T} \int_0^T x_{N/2}(t) dt = \frac{1}{a+b+1} \quad (4)$$

is the mean value of x_i and is equal to $1/3$ for all i when $s = a = b = 1$. The correlation function is plotted versus Δi in Fig. 6 with $s = 1$ and $N = 100$ for $\Delta t = 0, 50$, and 100 . This plot shows how the structure propagates and disperses, such that after a time of $\Delta t = 100$, very little correlation remains. The propagation velocity is consistent with $di/dt \cong 1/8$, and the correlation time is consistent with the inverse of the entropy, which is about $1/K \cong 61$ for this case.

4. Temporal Behavior

Figure 7 shows the temporal behavior of the biomass

$$M = \frac{1}{N} \sum_{i=1}^N x_i \quad (5)$$

biodiversity [24]

$$D = 1 - \frac{1}{2(N-1)} \sum_{i=1}^N \left| \frac{x_i}{M} - 1 \right| \quad (6)$$

and a typical x_i for the case with $N = 100$ and $s = 1$, illustrating the chaotic dynamics. The biomass fluctuates slightly about the equilibrium with $M = 1/(2s + 1)$, and the

biodiversity remains relatively high but has variations on the order of 10%. The biomass and the individual x_i values have a temporal average of $1/(2s + 1)$ as indicated in Eq. (4). Fluctuations in the biomass and biodiversity are suggestive of sporadic volatility and punctuated equilibria [25].

There are a number of dominant frequencies evident in the various signals, the most obvious of which is the oscillation in x_1 at a frequency of $\omega \cong 1/3$, which is the order of the linear frequency of the most unstable eigenvalue of the coexisting equilibrium as shown in Fig. 1, for which $\omega \cong 0.4834456$. By contrast, the biomass and biodiversity have a more broadband power spectrum, although they have a dominant component at $\omega \cong 1$, which is most evident if the low frequencies are suppressed by taking the time derivative of the signals.

5. Discussion

The system described here may be a minimal high-dimensional hyperchaotic Lotka-Volterra model in the sense of being the algebraically simplest such system. It is apparently prototypical of more complicated models and easily generalized to arbitrary dimension. It was motivated more by its elegant simplicity than by its realism as a model of any particular natural dynamical system. However, there may be situations in which agents are disinclined to compete with their nearest neighbors, who might for example be close relatives, and instead compete most strongly with the second nearest neighbors, at least in one direction.

The system is mathematically interesting because it can produce such a wide range of dynamical behaviors including equilibria, invariant loops, limit cycles, 2-tori, 3-tori, and strange attractors, with well-defined bifurcation points and linear frequencies. Solutions are automatically bounded in the range $[0, 1]$ for all agents, and most cases have a single attractor, implying that initial conditions are arbitrary. It is suitable for studying temporal transients, routes to chaos, dimensionality scaling, synchronization, structural stability, and robustness. Its spatiotemporal nature allows it to exhibit self-organization, pattern formation, and spontaneous symmetry breaking.

The model can be extended to more realistic two (or even three) spatial dimensions by weakly coupling many identical one-dimensional rows of these systems, forming a torus in space. It can be generalized to the case $a \neq b$. Finally, it is very useful for studying the effect of network architecture on the dynamics since (for $a = b = 1$) all connected nodes have identical unit strength, and the connections can thus be rearranged without regard to their magnitude. The system is ripe for further study.

Acknowledgments

We are grateful to David Albers, Mike Anderson, Jeff Noel, and John Vano for helpful discussion.

References

- [1] Lotka AJ. Elements of physical biology. New York: Williams and Wilkins, 1925.
- [2] Volterra V. Variazioni e fluttuazioni del numero d'individui in specie animali conviventi. Mem. Acad. Lincei. 1926;2:31–113.
- [3] Murray JD. Mathematical biology 2nd edn. New York: Springer, 1993.
- [4] Asai T, Ohtani M, Yonezu H. Analog integrated circuits for the Lotka-Volterra competitive neural networks. IEEE Trans. Neural Networks 1999;10:1222–31.
- [5] McArthur RH. Species packing and competitive equilibrium for many species. Theor. Pop. Biol. 1970;1:1–11.
- [6] Davis PJ. Circulant matrices, 2nd edn. New York: Chelsea, 1994.
- [7] Verhulst PF. Recherches mathématiques sur la loi d'accroissement de la population. Nouveaux Memoires de l'Academic Royale des Sciences et Belles-Lettres de Bruxelles 1845;18:1–45.
- [8] Wildenberg JC, Sprott JC, Vano JA. Animated eigenvalues for a simple Lotka-Volterra model. <http://sprott.physics.wisc.edu/chaos/eigenz.gif>.
- [9] Sprott JC. Chaos and time-series analysis. Oxford: Oxford University Press, 2003, pp. 116–7.
- [10] Kaplan J, Yorke J. Chaotic behavior in multidimensional difference equations. In Functional Differential Equations and Approximation of Fixed Points, Lecture Notes in Mathematics, Vol. 730 (ed. H. -O. Peitgen & H. -O. Walther). Berlin: Springer, 1979, pp. 228-37.

- [11] Ruelle D, Takens F. On the nature of turbulence. *Comm. Math. Phys.* 1971;20:167–92.
- [12] Sprott JC. *Strange Attractors: Creating Patterns in Chaos*. New York: M&T Books, 1993.
- [13] Marsden JE and McCracken M. *The Hopf bifurcation and its applications*. New York: Springer, 1976.
- [14] Grebogi C, Ott E, Yorke JA. Are three frequency orbits to be expected in typical nonlinear dynamical systems? *Phys. Rev. Lett.* 1983;51:339–42.
- [15] Grebogi C, Ott E, Yorke JA. Attractors on an N-torus: quasiperiodicity versus chaos. *Physica D* 1985;15:354–73.
- [16] Ruelle D and Takens F. On the nature of turbulence. *Commun. Math. Phys.* 1971;20:167–92.
- [17] Pesin YaB. Characteristic Lyapunov exponents and smooth ergodic theory. *Russian Math. Surveys* 1977;32:55–114.
- [18] Sompolinsky H, Crisanti A, Sommers HJ. Chaos in random neural networks. *Phys. Rev. Lett.* 1988;61:259–62.
- [19] Albers DJ, Sprott JC, Dechert WD. Routes to chaos in neural networks with random weights. *Int. J. Bifur. Chaos* 1988;8:1463–78.
- [20] Aronson DG, Chory MA, Hall GR, McGehee RP. Bifurcations from an invariant circle for two-parameter families of maps of the plane: a computer-assisted study. *Comm. Math. Phys.* 1982;83:304–54.
- [21] Turing AM. The chemical basis of morphogenesis. *Philos. Trans. R. Soc. London B* 1952;237:37–72.

[22] Meinhardt H. Models of biological pattern formation. New York: Academic Press, 1982.

[23] Brading K and Castellani E (eds.). Symmetries in physics: philosophical reflections. Cambridge: Cambridge University Press, 2003.

[24] Sprott JC. Competition with evolution in ecology and finance. Phys. Lett. A 2004;325:329–33.

[25] Gould SJ and Eldridge N. Punctuated equilibrium: the tempo and mode of evolution reconsidered. Paleobiology 1977;3:115–51.

Table I. Route to chaos for increasing N with $a = b = 1$ in Eq. (2).

N	Attractor	D	Comment
1	Equilibrium	0	
2	Equilibrium	0	
3	Invariant loop	1	Hopf, $\omega = 1/\sqrt{3}$
4	Equilibrium	0	Hopf, $\omega = 1/3$
5	Equilibrium	0	
6	Invariant loop	1	Hopf, $\omega = 1/\sqrt{3}$
7	Limit cycle	1	
8	Equilibrium	0	Hopf, $\omega = 1/3$
9	Invariant loop	1	Hopf, $\omega = 1/\sqrt{3}$
10	2-torus	2	
11	2-torus	2	
12	Equilibrium	0	Hopf-Hopf, $\omega = 1/3, 1/\sqrt{3}$
13	2-torus	2	
14	2-torus	2	
15	2-torus	2	
16	3-torus	3	
17	2-torus	2	
...	All 2-tori
45	2-torus	2	
46	3-torus	3	
47	2-torus	2	
48	2-torus	2	
49	2-torus	2	
50	3-torus	3	
51	3-torus	3	
52	2-torus	2	
53	2-torus	2	
54	3-torus	3	Highly crinkled torus
...	All 3-tori
58	3-torus	3	
59	Chaotic	4.2022...	
60	Chaotic	4.0381...	
61	3-torus	3	
62	3-torus	3	
63	Chaotic	6.5480...	
64	Chaotic	6.1306...	
65	3-torus	3	
66	Chaotic	4.4777...	
...	...	>4	All chaotic

Figure Captions

Fig. 1. Eigenvalues of the coexisting equilibrium with $N = 100$ and $s = 1$.

Fig. 2. A one-dimensional ring of species interacting according to Eq. (2).

Fig. 3. Largest Lyapunov exponent and Kaplan-Yorke dimension for Eq. (2) with $s = 1$.

Fig. 4. Largest Lyapunov exponent for Eq. (2) with $N = 100$ showing the quasiperiodic route to chaos that is typical of high-dimensional systems.

Fig. 5. Spatiotemporal plot of $|x_{i+1} - x_i|$ from Eq. (2) with $N = 480$ and $s = 1$.

Fig. 6. Spatiotemporal cross-correlation function with $N = 100$ and $s = 1$ showing propagation and dispersion.

Fig. 7. Total biomass, biodiversity, and a typical $x(t)$ versus time for Eq. (2) with $N = 100$ and $s = 1$.

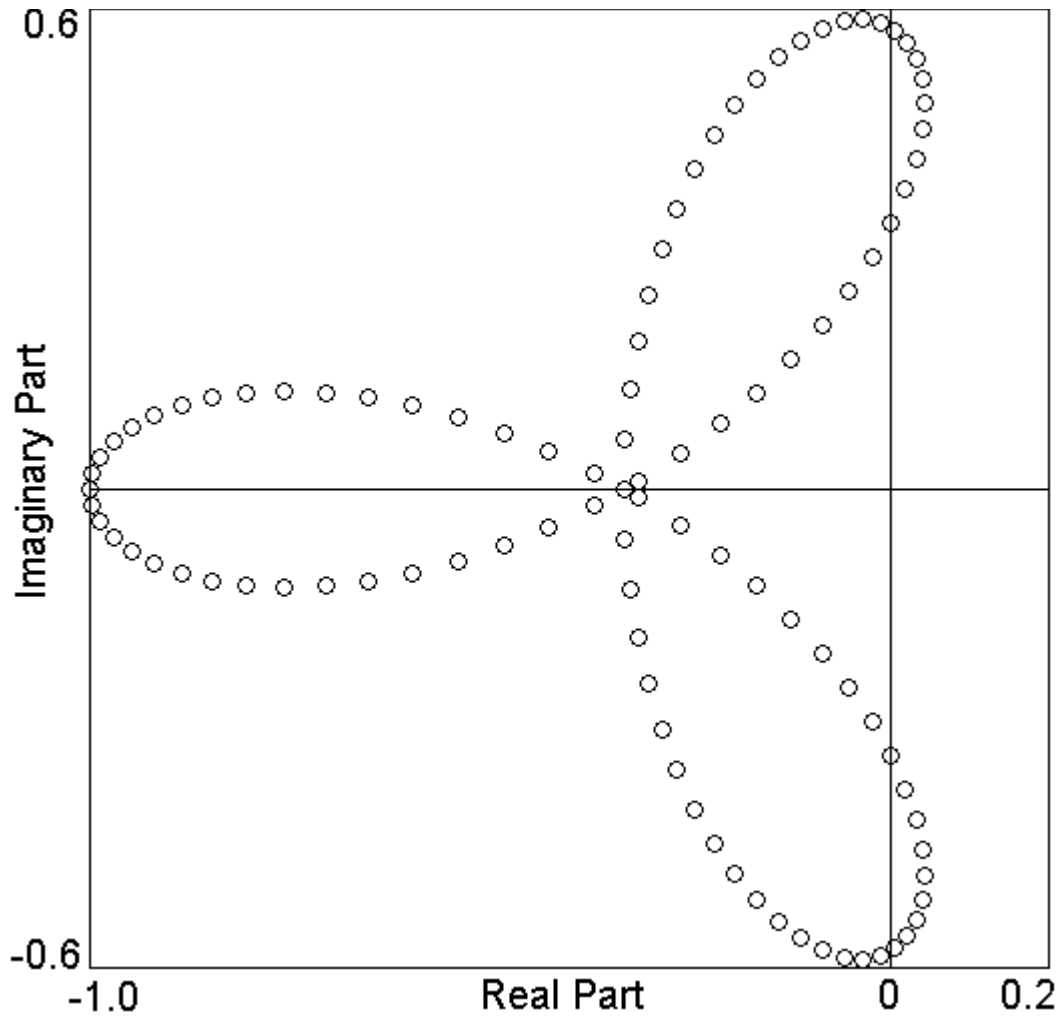


Fig. 1. Eigenvalues of the coexisting equilibrium with $N = 100$ and $s = 1$.

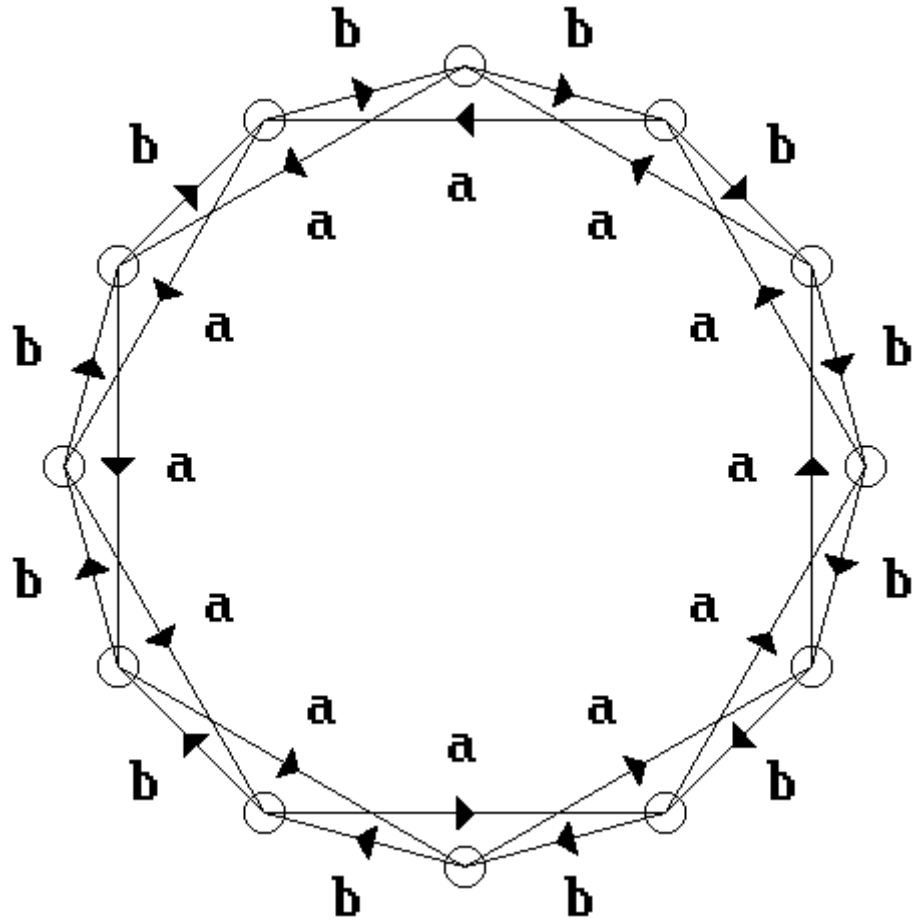


Fig. 2. A one-dimensional ring of species interacting according to Eq. (2).

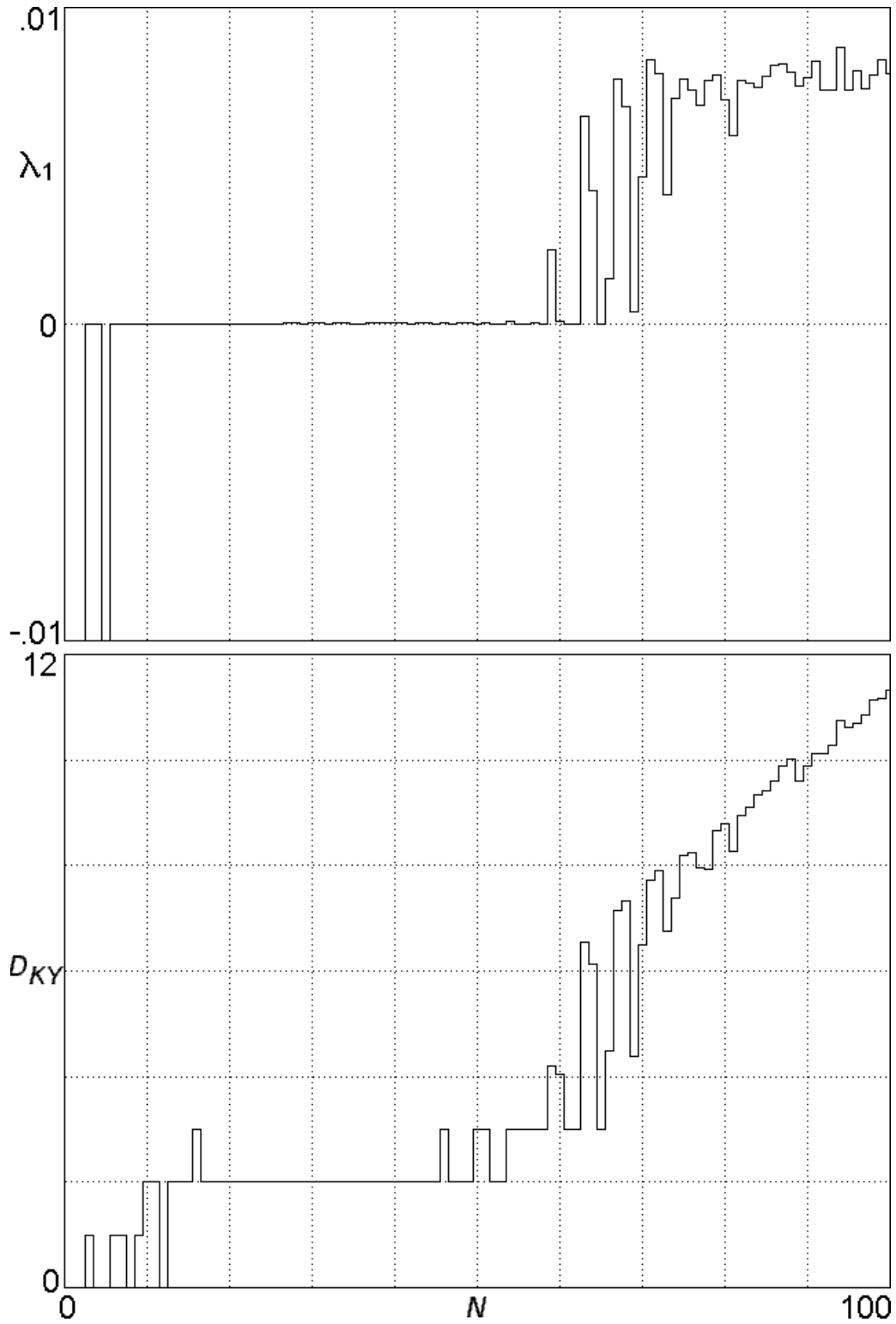


Fig. 3. Largest Lyapunov exponent and Kaplan-Yorke dimension for Eq. (2) with $s = 1$.

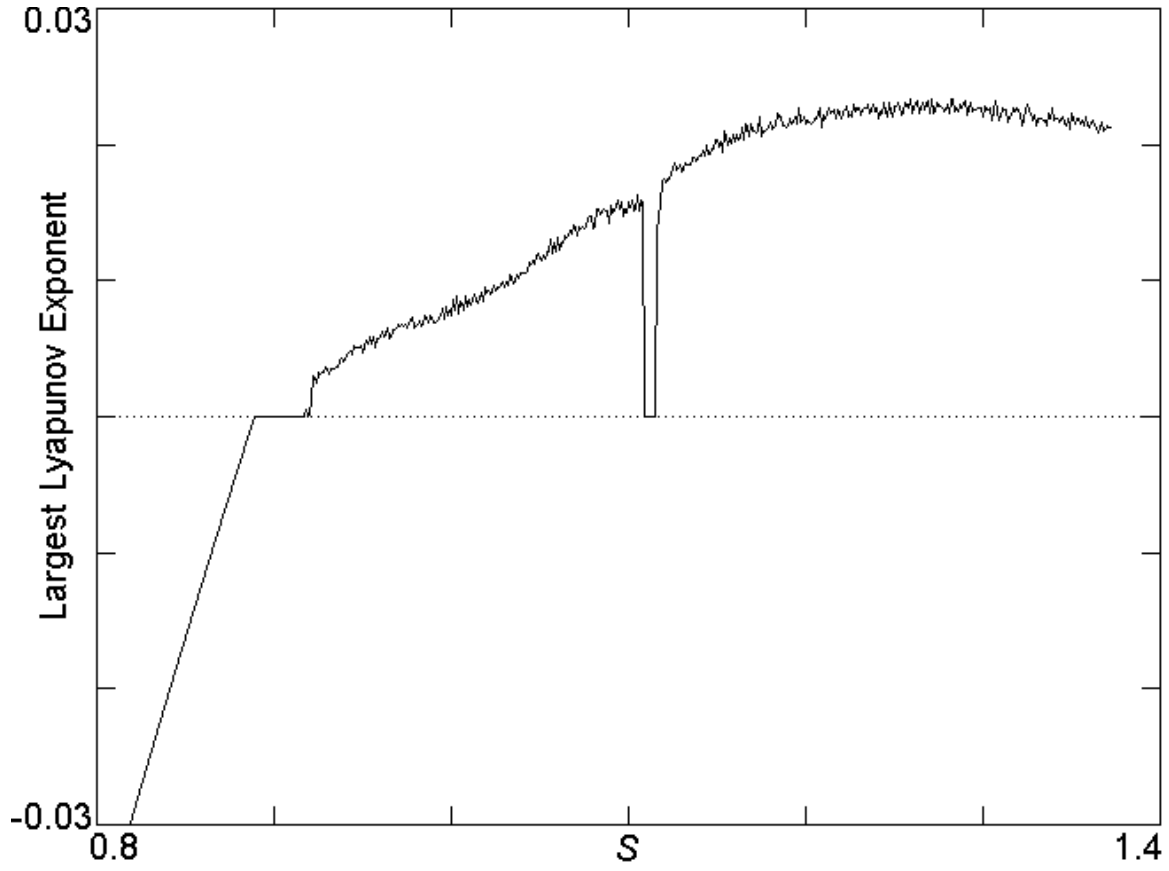


Fig. 4. Largest Lyapunov exponent for Eq. (2) with $N = 100$ showing the quasiperiodic route to chaos that is typical of high-dimensional systems.

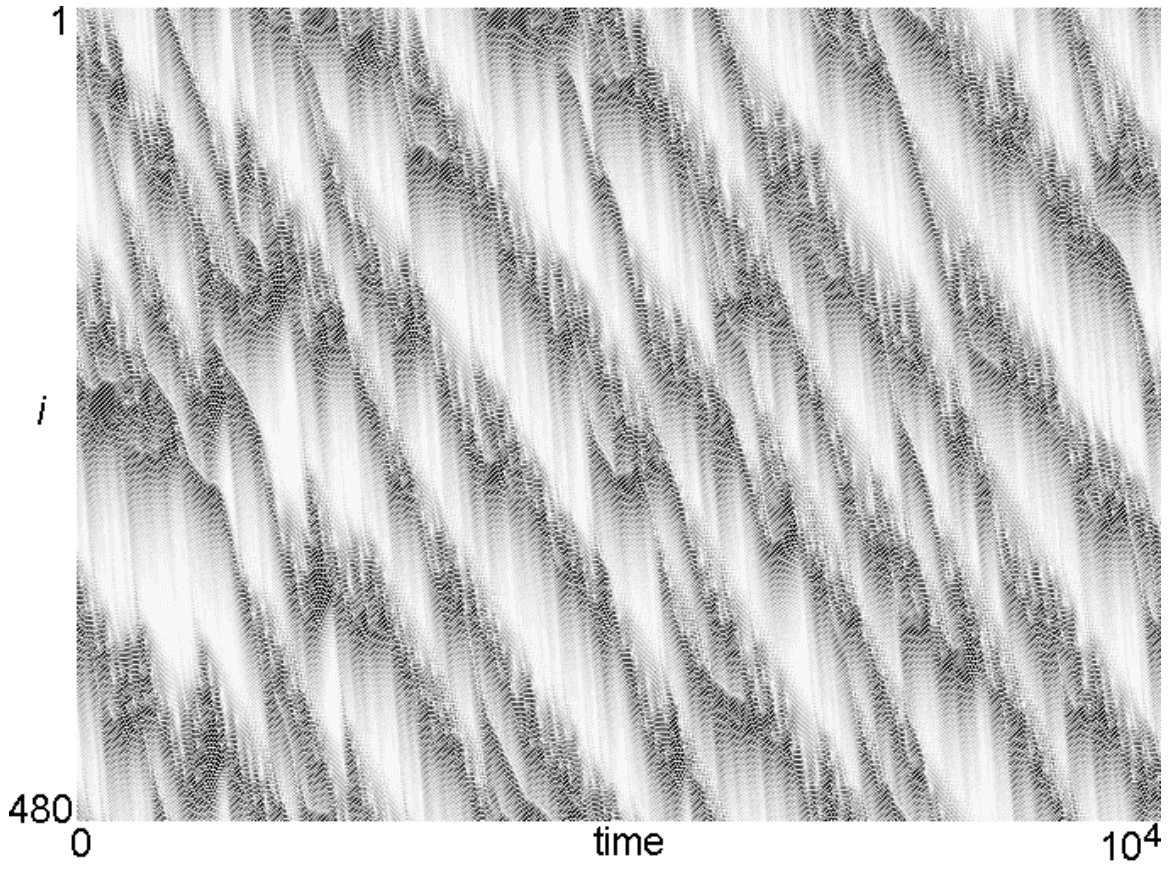


Fig. 5. Spatiotemporal plot of $|x_{i+1} - x_i|$ from Eq. (2) with $N = 480$ and $s = 1$.

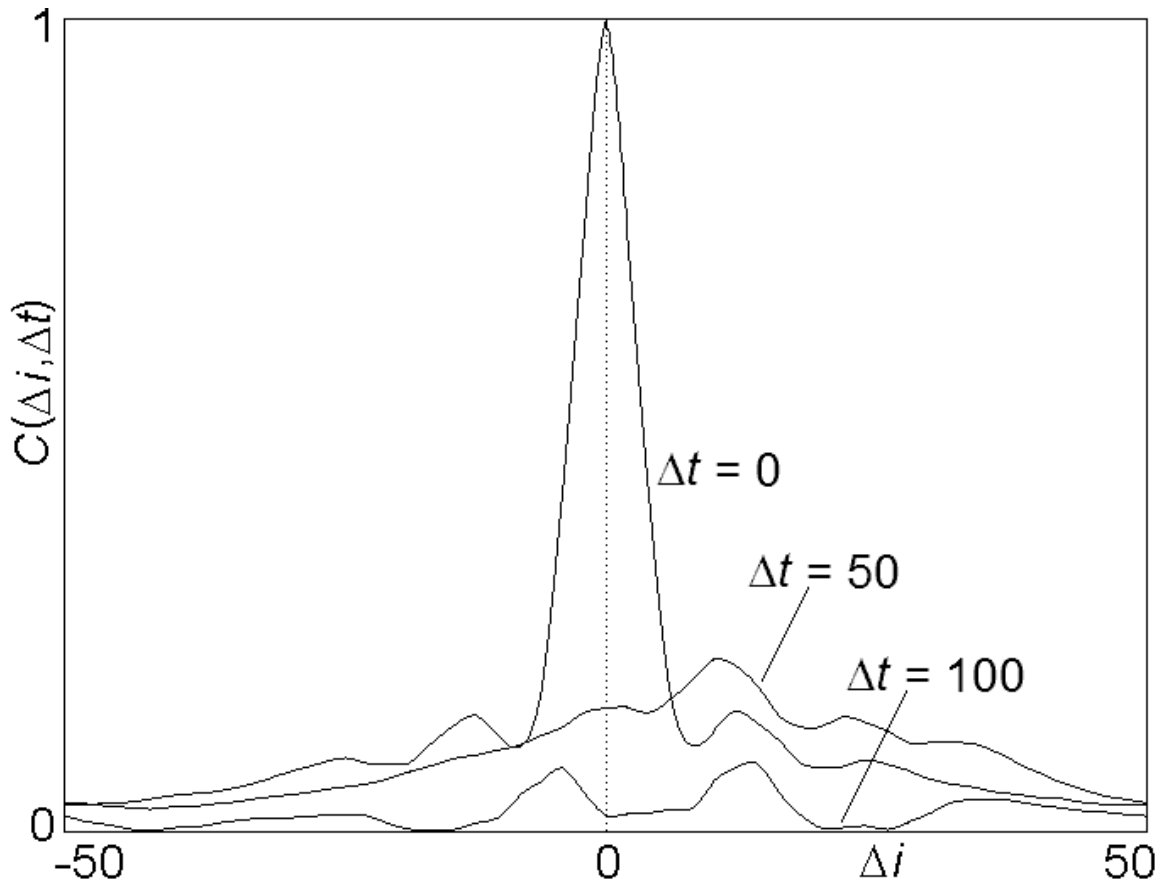


Fig. 6. Spatiotemporal cross-correlation function with $N = 100$ and $s = 1$ showing propagation and dispersion.

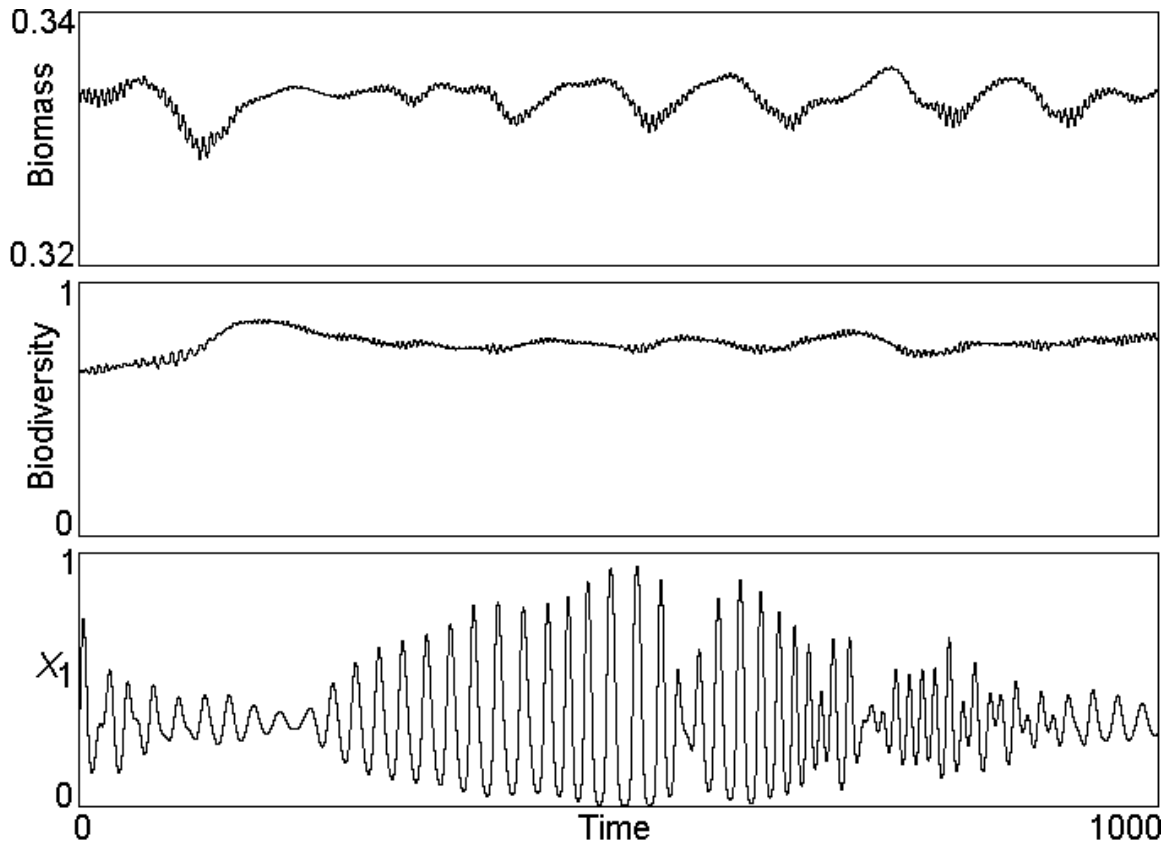


Fig. 7. Total biomass, biodiversity, and a typical $x(t)$ versus time for Eq. (2) with $N = 100$ and $s = 1$.